ARTICLE
Journal of Cellular Biochemistry 111:1413–1425 (2010)

Journal of Cellular Biochemistry

Changes in Cell Adhesivity and Cytoskeleton-Related Proteins During Imatinib-Induced Apoptosis of Leukemic JURL-MK1 Cells

K. Kuželová,[1*] M. Pluskalová,[1] D. Grebeňová,[1] K. Pavlásková,[2] P. Halada,[2] and Z. Hrkal[1]

[1]*Department of Cellular Biochemistry, Institute of Hematology and Blood Transfusion, Prague, Czech Republic*

[2]*Laboratory of Mass Spectrometry, Institute of Microbiology of the ASCR, v.v.i., Prague, Czech Republic*

ABSTRACT

The fusion protein Bcr–Abl, which is the molecular cause of chronic myelogenous leukemia (CML) interacts in multiple points with signaling pathways regulating the cellular adhesivity and cytoskeleton architecture and dynamics. We explored the effects of imatinib mesylate, an inhibitor of Bcr–Abl protein used in front-line CML therapy, on the adhesivity of JURL-MK1 cells to fibronectin and searched for underlying changes in the cell proteome. As imatinib induces apoptosis of JURL-MK1 cells, we used three different caspase inhibitors to discriminate between direct consequences of Bcr–Abl inhibition and secondary changes related to the apoptosis. Imatinib treatment caused a transient increase in JURL-MK1 cell adhesivity to fibronectin, possibly due to the switch off of Bcr–Abl activity. Subsequently, we observed a number of changes including a decrease in cell adhesivity, F-actin decomposition, reduction of integrin β1, CD44, and paxillin expression levels and a marked increase in cofilin phophorylation at Ser3. These events were generally related to the proceeding apoptosis but they differed in their sensitivity to the individual caspase inhibitors. J. Cell. Biochem. 111: 1413–1425, 2010.

KEY WORDS: IMATINIB; ADHESION; CYTOSKELETON; APOPTOSIS; Q-VD-OPH; COFILIN; JURL-MK1

Hematopoietic cell adhesion to the bone marrow is mainly mediated by interaction of integrins and other cell surface receptors with protein components of the extracellular matrix (ECM), such as fibronectin. These interactions not only retain the unmature cell in the bone marrow microenvironment where it is exposed to appropriate regulatory substances but also regulate the activity of different intracellular signal cascades that consequently modulate diverse cellular functions including the cell proliferation, migration, or apoptosis. Alterations of these signaling pathways are commonly found in neoplastic cells. Chronic myelogenous leukemia (CML) is a myeloproliferative disorder, which is initiated by chromosomal translocation resulting in the formation of the fusion Bcr–Abl gene [Goldman and Melo, 2003]. Bcr–Abl protein expression affects in multiple points the pathways mediating the signaling from integrins (focal adhesion pathways), both through its constitutive tyrosine-kinase activity and through domains regulating the activity of small Rho GTPases, the key molecules in the control of the architecture and dynamics of the cell cytoskeleton [Zandy et al., 2007; Vega and Ridley, 2008]. As the interaction of Bcr–Abl with focal adhesion signaling is complex, the resulting effect of Bcr–Abl expression on the cell adhesion is unpredictable and depends on the cellular context [Kuželová and Hrkal, 2008]. To date, the experimental analysis of Bcr–Abl effects on the cell adhesion to the bone marrow components (usually to fibronectin) have revealed both elevated and attenuated adhesion in different Bcr–Abl expressing cell types [Bazzoni et al., 1996; Salgia et al., 1997; Bhatia and Verfaillie, 1998; Kramer et al., 1999; Gaston et al., 2000; Zhao et al., 2001; Cheng et al., 2002; Salesse and Verfaillie, 2002; Wertheim et al., 2002, 2003; Ramaraj et al., 2004]. Barnes et al. (2005) have found that the final effect of Bcr–Abl expression on the adhesion of Bcr–Abl-transfected 32D cells depends on the amount of the fusion protein. Nevertheless, from our experience, Bcr–Abl expression level does not correlate with the cell adhesivity to fibronectin for different CML cell lines (our unpublished observation). Another possible source of variability in the experimental results is the fact that Bcr–Abl inhibition triggers

Additional supporting information may be found in the online version of this article.

Grant sponsor: Ministry of Health of the Czech Republic; Grant numbers: NR 9243-3, VZ 00023736; Grant sponsor: Ministry of Education, Youth and Sports of the Czech Republic; Grant numbers: LC 07017, AV0Z50200510.

*Correspondence to: K. Kuželová, Institute of Hematology and Blood Transfusion, U Nemocnice 1, 128 20 Prague 2, Czech Republic. E-mail: kuzel@uhkt.cz

Received 31 March 2010; Accepted 25 August 2010 • DOI 10.1002/jcb.22868 • © 2010 Wiley-Liss, Inc.
Published online 9 September 2010 in Wiley Online Library (wileyonlinelibrary.com).

apoptosis in the majority of CML cells. It is known that the apoptosis includes an early cell detachment from the environment and complex rearrangements of the actin cytoskeleton leading to the initial cell contraction and rounding, formation of membrane blebs, and eventual cell breakdown into apoptotic bodies [Coleman and Olson, 2002].

In the present work, we analyzed the changes in the cell adhesivity to fibronectin and in actin polymerization upon treatment of the CML cell line JURL-MK1 with the inhibitor of Bcr–Abl tyrosine kinase activity, imatinib mesylate. We compared the proteomes of control and treated cells and focused on the behavior of the proteins, which are known to be involved in the regulation of cytoskeleton dynamics and cell adhesivity. To characterize potential contribution of apoptotic processes, we used three caspase inhibitors, which differ in their ability to prevent various stages of the apoptosis.

MATERIALS AND METHODS

CHEMICALS

Imatinib mesylate was kindly provided by Novartis (Basel, Switzerland). The stock solution (10 mM) was prepared by dissolving imatinib mesylate in sterile distilled water and stored at minus 20°C. Human fibronectin (alpha-chymotryptic fragment, 120 K) and the labeled antibody against integrin β1 (CD29) were purchased from Chemicon International (CA). Caspase inhibitors zDEVDfmk, zVADfmk, and Q-VD-OPh were from Sigma (Prague, Czech Republic), Alexis Biochemicals (Lausen, Switzerland), and R&D Systems (Minneapolis), respectively. The inhibitor Y-27632, which inhibits ROCK1 and ROCK2 was from Calbiochem. Anti-β-actin antibody (cat. no A 5441), anti-Rho-GDI (cat. no R 3025), FITC-labeled phalloidin, and the fluorogenic substrate Ac-DEVD-AFC were obtained from Sigma, anti-paxillin (clone 5H11) and anti-ROCK1 (cat. no 07–903) antibodies from Millipore (Upstate). Anti-phospho-cofilin (pSer3, cat. no C8992), anti-tropomyosin3 (Sigma Prestige Antibodies™), and anti-tropomyosin4 antibodies were obtained from Sigma, anti-cofilin antibody from Chemicon International (cat. no AB3842), anti-tropomyosin1 (alpha) antibody from Abcam (Cambridge), anti-Bcr (cat. no sc-103) antibody, and FITC-conjugated anti-rabbit IgG (cat. no sc-2012) from Santa Cruz Biotechnology, Alexa Fluor 546-conjugated anti-rabbit IgG from Invitrogen (Mol. Probes, cat. no A11010), PE-conjugated anti-CD44 (cat. no MHCD4404) and anti-CD62P (cat. no MHCD6204) also from Invitrogen (Camarillo, CA). PE-conjugated anti-CD62L (cat. no 12–0629–73) was from eBiosciences. Rabbit polyclonal antibodies against LIMK1 (cat. no 3842) and against PAK1 (cat. no 2601) were from Cell Signaling Technology®.

CELL CULTURE

JURL-MK1 cells derived from a patient with CML were purchased from DSMZ (German Collection of Microorganisms and Cell Cultures, Braunschweig, Germany). The cells were cultured in RPMI 1640 medium supplemented with 10% fetal calf serum, 100 U/ml penicillin, and 100 μg/ml streptomycin at 37°C in 5% CO_2 humidified atmosphere.

CASPASE ACTIVITY

The activity of caspase-3 was determined by fluorometric measurement of the kinetics of 7-amino-4-trifluoromethyl coumarin (AFC) release from the fluorogenic substrate Ac-DEVD-AFC in the presence of cell lysates. The method was described in detail in Kuželová *et al.*, 2007. After the incubation with effectors the cells were washed and lysed and aliquots of cytosolic fractions were incubated for 30 min at 37°C with the fluorogenic substrate. The linear increase of fluorescence intensity at 520 nm was monitored during this incubation time using Fluostar Galaxy microplate reader (BMG Labtechnologies, Germany).

FLOW CYTOMETRY ANALYSIS

Flow cytometry measurements were performed on Coulter Epics XL flow cytometer.

The fraction of cells containing apoptotic DNA breaks was measured by TUNEL assay using the in situ Cell Death Detection Kit, Fluorescein (Roche Diagnostics GmbH, Mannheim, Germany) following the standard manufacturer's protocol.

To analyze the expression level of integrin β1 or CD44 on the cell surface, the cells (5×10^5) were washed in PBS and stained with 5 μl PE-conjugated anti-integrin β1 or anti-CD44. After 40 min incubation at room temperature, the cells were washed twice in PBS and the fluorescence histograms of PE fluorescence were recorded using the flow cytometer.

To stain the actin polymers, the cells were washed in PBS and fixed and permeabilized using FIX&PERM cell permeabilization kit from An Der Grub (Kaumberg, Austria). Washing steps were performed in PBS supplemented with 1% BSA using short centrifugation times (2 min at 350 g). FITC-labeled phalloidin (3 μl) was added to cells suspended in 50 μl PERM solution. The samples were incubated for 40 min at room temperature, washed in PBS + 1% BSA and the green fluorescence was measured using the flow cytometer.

ADHESION ASSAY

The extent of JURL-MK1 cell adhesion to fibronectin was measured using the previously described protocol [Kuželová *et al.*, 2010]. Briefly, the cells were applied to fibronectin-coated wells of a microtitration plate and incubated for 1 h at 37°C. Then, the wells were washed with PBS/Ca^{2+}/Mg^{2+} using a multichannel adaptor to the succion pump and the remaining cells were quantified by means of fluorescent labeling (Cy-Quant Cell Proliferation Assay Kit; Molecular Probes). The adherent cell fraction (ACF) was calculated using the fluorescence signal from fibronectin-coated plate and that from reference plate, which contained the total cell number.

1-D ELECTROPHORESIS AND WESTERN-BLOTTING

Control and treated cells (3×10^6) were washed twice in PBS, suspended in 150 μl lysis buffer (300 mM NaCl, 50 mM Tris–HCl pH 8.0, 5 mM EDTA, 1 mM DTT, 1 mM PMSF, 1% NP-40, phosphatase inhibitor coctail 5 μl per 2×10^7 cells, protease inhibitor coctail 4 μl per 2×10^7 cells) and kept for 30 min on ice. The protein concentration was measured using a BioRad protein assay (BioRad Hercules, CA). Protein samples were heated to 100°C for 4 min in the presence of 5% 2-mercaptoethanol, chilled and subjected to one-dimensional electrophoresis (PAGE) in 6, 12, or 15% gel with SDS. As a rule, 15 μg total protein was applied to each well. Proteins were transferred to Hybond-ECL membrane at 90 V for 1–2 h (wet transfer).

Nitrocellulose membranes were blocked with 5% non-fat milk or 3% BSA in TBS-T (Tris-buffered saline, 0.1% Tween-20) for 1 h at room temperature, incubated with the appropriate antibody in TBS-T solution (1 h at room temperature or overnight at 4°C), washed in TBS-T and incubated with the horseradish peroxidase-conjugated anti-mouse or anti-rabbit secondary antibody. The antigens were detected using SuperSignal® West Pico Chemiluminiscent Substrate (Pierce Biotechnology, IL) according to the manufacturer's instructions and visualized by autoradiography on X-ray film. Immunoblots were reacted in parallel with anti-β-actin as a control of the equal protein loading. The protein bands were evaluated by densitometry using AIDA version 4.08 (Raytest, Germany).

2-D ELECTROPHORESIS

The linear immobilized pH gradient gels ($180 \times 3.3 \times 0.5\ mm^3$), ReadyStrip™ IPG strips pH 3–10 (BioRad), were rehydrated overnight in 315 μl of the cell lysate containing 1 mg proteins, 7 M urea, 2 M thiourea, 1.2% CHAPS, 0.5% ASB-14, 30 mM Tris, 43 mM DTT, 0.2% Bio-Lyte 3–10. Isoelectric focusing (IEF) was performed using Protean IEF Cell instrument (BioRad) at 6,000 V for a total 40–60 kVh at 20°C. After the first dimension run, the strips were equilibrated with a solution containing Tris–HCl pH 8.8 (0.375 mM), urea (6 M), glycerol (20% v/v), DTT (2% w/v), SDS (2% w/v), and 0.01% bromphenol blue. Resulting free SH groups were blocked in the second equilibration step in which DTT was replaced with iodoacetamide (2.5% w/v).

The second dimension run was performed using a Protean II xi vertical electrophoresis system (BioRad), gel size $200 \times 200 \times 1\ mm^3$, in a Laemmli–SDS discontinuous buffer system and polyacrylamide gel gradient (9–16% T, 2.6% C). The equilibrated first dimension gel was placed directly onto the second dimension gel and overlaid with a solution containing 0.4% agarose in Tris–glycine–SDS pH 8.3 buffer (25 mM Tris, 192 mM glycine, 0.1% w/v SDS) heated to 70°C. Electrophoresis was performed at a constant current 35 mA/gel for 5 h at 10°C. The gels were fixed in a solution containing ethanol (40% v/v) and acetic acid (10% v/v) before staining. The gels were stained with Coomassie blue (CBB), scanned and analyzed employing Phoretix® 2D Expression Software (Nonlinear Dynamics, UK, version 2005). The selected protein spots were excised from the gel and subjected to MALDI-TOF MS analysis.

ENZYMATIC IN-GEL DIGESTION

CBB-stained protein spots were excised from the gel, cut into small pieces and destained with 50 mM 4-ethylmorpholine acetate (pH 8.1) in 50% acetonitrile (MeCN). After complete destaining, the gel was washed with water, shrunk by dehydration in MeCN and reswelled again in water. The supernatant was removed and the gel was partly dried in a SpeedVac concentrator. The gel pieces were then rehydrated in a cleavage buffer containing 25 mM 4-ethylmorpholine acetate, 5% MeCN and trypsin (100 ng; Promega), and incubated overnight at 37°C. The resulting peptides were extracted to 40% MeCN/0.1% TFA. An aqueous 50% MeCN/0.1% TFA solution of α-cyano-4-hydroxycinnamic acid (5 mg/ml; Sigma) was used as a MALDI matrix. The sample (0.5 μl) was deposited on the MALDI target and allowed to air-dry at room temperature. After complete evaporation, 0.5 μl of the matrix solution was added. If necessary, the peptides were desalted and concentrated using a GELoader microcolumn (Eppendorf, Hamburg, Germany) packed with a Poros Oligo R3 material [Larsen *et al.*, 2005]. The purified peptides were eluted from the microcolumn in

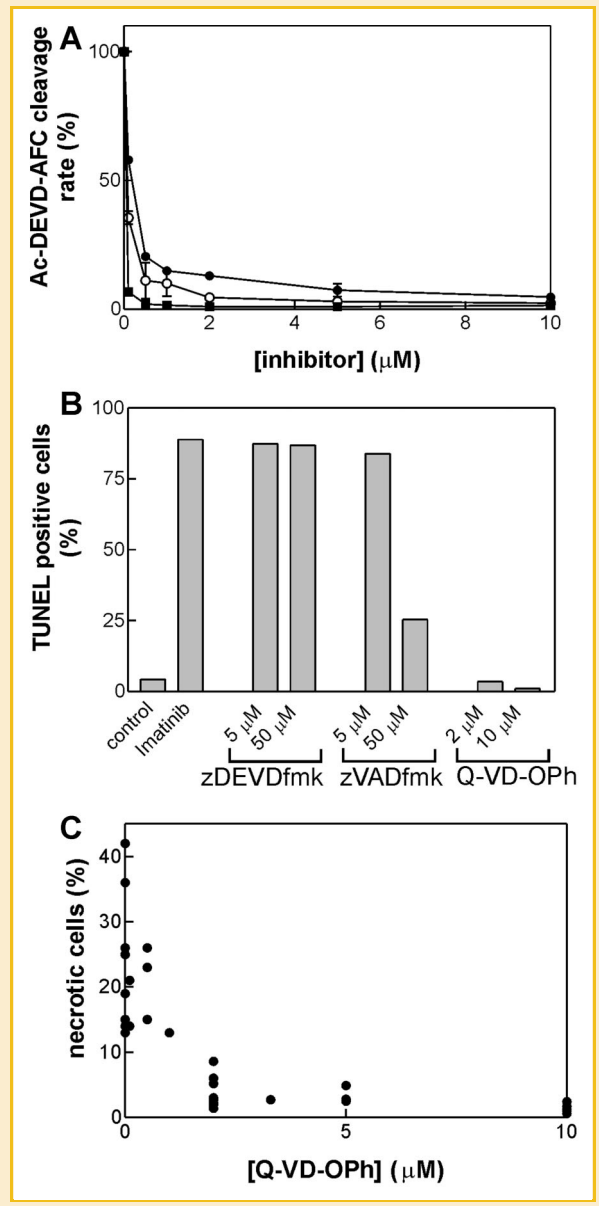

Fig. 1. The effect of caspase inhibitors on caspase-3 activity, apoptotic DNA fragmentation and cell death in imatinib-treated JURL-MK1 cells. The cells were treated with 1 μM imatinib alone or in combination with different concentration of zDEVDfmk, zVADfmk, or Q-VD-OPh as indicated. A: After 42 h incubation, the cells were harvested and the activity of caspase-3 in the cell lysate was measured using the fluorogenic caspase-3 substrate Ac-DEVD-AFC. Imatinib mesylate alone induced about 7–15 fold increase in caspase-3 activity over the controls. The given values of caspase-3 activity are relative to those from samples treated with imatinib only. Symbols: zDEVDfmk—open circles, zVADfmk—closed circles, Q-VD-OPh—squares. B: After 48 h incubation, the cells were harvested and the apoptotic DNA breaks were stained using TUNEL method. C: Fraction of Trypan blue-positive cells after 42–48 h incubation with imatinib alone or in combination with Q-VD-OPh at different concentrations. The points correspond to individual experiments.

several droplets directly onto MALDI plate using 1 μl of the matrix solution. The phosphopeptide enrichment was performed as described previously [Larsen *et al*., 2005].

MALDI-TOF MASS SPECTROMETRY (MS) AND PROTEIN IDENTIFICATION

Mass spectra were measured on an Ultraflex III MALDI-TOF/TOF instrument (Bruker Daltonics, Bremen, Germany) equipped with a Smartbeam™ solid state laser and LIFT™ technology for MS/MS analysis. The spectra were acquired in the mass range of 700–4,000 Da and calibrated externally using peptide calibration mix II (Bruker Daltonics).

For PMF database searching, peak lists in XML data format were created using flexAnalysis 3.0 program with SNAP peak detection algorithm. No smoothing was applied and maximal number of assigned peaks was set to 50. After peak labeling all known contaminant signals were removed. The peak lists were searched using in-house MASCOT search engine against SwissProt 57.13 database subset of human proteins with the following search settings: peptide tolerance of 30 ppm, missed cleavage site value set to two, variable carbamidomethylation of cysteine, oxidation of methionine, and protein N-term acetylation. No restriction on protein molecular weight and pI value were applied. Proteins with MOWSE score over the threshold 56 calculated for the used settings were considered as identified. If the score was lower or only slightly higher than the threshold value, the identity of protein candidate was confirmed by MS/MS analysis. In addition to the above mentioned MASCOT settings fragment mass tolerance of 0.6 Da and instrument type MALDI-TOF-TOF was applied for MS/MS spectra searching.

IMMUNOFLUORESCENCE MICROSCOPY

JURL-MK1 cells were incubated with 1 μM imatinib mesylate for 40 h. Control and imatinib-treated cells were collected by

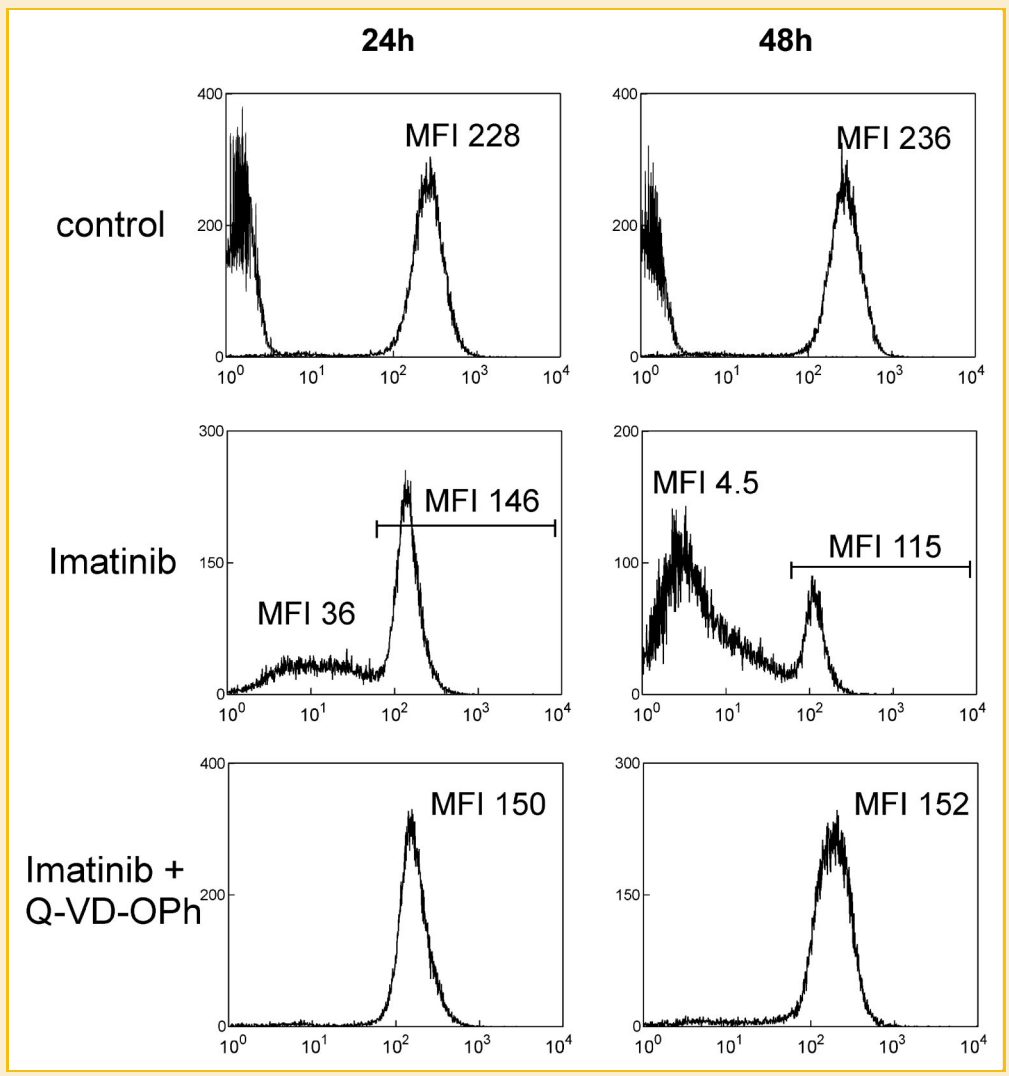

Fig. 2. F-actin depolymerization due to imatinib treatment of JURL-MK1 cells. The cells were treated with 1 μM imatinib mesylate alone or in combination with 2 μM Q-VD-OPh for 24 or 48 h as indicated. F-actin was labeled using FITC-phalloidin and quantified using flow-cytometry. MFI stands for mean fluorescence intensity. Negative controls (no staining) are shown on the left side of the upper panels. Three additional experiments yielded closely similar results.

centrifugation, washed in PBS, and plated on glass coverslips. Cells were fixed with 3% paraformaldehyde in PBS for 15 min and permeabilized with 0.3% Triton X-100 in PBS for 10 min. After blocking with 3% bovine serum albumin in PBS supplemented with 0.03% Tween-20 for 10 min, cells were stained with primary antibody at 37°C for 1 h. Antibodies were diluted in blocking buffer and dilutions were as follows; anti-pSer3-cofilin antibody 1:100, anti-cofilin 1:200. Subsequently, cells were washed three times with 0.1% Tween 20 in PBS for 10 min and stained with secondary antibody for 1 h (FITC-conjugated anti-rabbit IgG for pSer3-cofilin or Alexa Fluor 546-conjugated anti-rabbit IgG for cofilin, both diluted 1:200 in blocking buffer). After washing with PBS–Tween, the coverslips were mounted using Vectashield (for cofilin staining) or Vectashield containing propidium iodide (for pSer3-cofilin). Images were obtained using inverted fluorescence microscope Olympus IX 81 with Cell-R system with magnification 60×. The green fluorescence intensity from individual cells was evaluated using Phoretics™ 2D Expression (Nonlinear Dynamics).

RESULTS

In agreement with previous studies involving other Bcr–Abl positive cells [Dai *et al.*, 2004], imatinib treatment of JURL-MK1 cells resulted not only in the inhibition of Bcr–Abl tyrosine kinase activity but also in a subsequent decrease of Bcr–Abl expression level: we observed a reduction by (56 ± 17)% after 24 h and by (88 ± 18)% after 48 h treatment with imatinib (mean and standard deviation from five experiments, Supplementary Material: Fig. 1S). We have previously shown that imatinib mesylate induces apoptosis including a marked caspase-3 activation and DNA fragmentation in JURL-MK1 cells [Kuželová *et al.*, 2005].

CHARACTERIZATION OF CASPASE INHIBITORS

In the present work, we used three different caspase inhibitors which differ in their specificity towards the individual caspases: zDEVDfmk is considered to be relatively specific for caspase-3, zVADfmk is a broad range caspase inhibitor and Q-VD-OPh is a new generation broad caspase inhibitor, which is claimed to be more specific for the caspase family, more potent and less toxic to the cells. Fig. 1 shows the effect of these inhibitors on caspase-3 activity (panel A) and DNA-fragmentation (panel B) in Imatinib mesylate-treated JURL-MK1 cells. As only Q-VD-OPh was able to completely inhibit apoptotic DNA fragmentation (no increase in TUNEL-positive cell fraction compared to the control samples occurred for up to 70 h when imatinib was added simultaneously with 10 μM Q-VD-OPh, data not shown), we used prevalently this inhibitor for subsequent studies. Q-VD-OPh also markedly reduced the fraction of dead (Trypan blue-positive) cells in imatinib-treated samples (Fig. 1C). In control JURL-MK1 cell samples, the fraction of Trypan blue-positive cells was usually about 2%.

F-ACTIN DISASSEMBLY

To assess changes in the amount of polymeric actin (F-actin), JURL-MK1 cells were stained with FITC-labeled phalloidin and measured using a flow-cytometry apparatus. As shown in Fig. 2, imatinib mesylate treatment first induced a homogeneous moderate decrease of actin polymerization, which was followed by massive decomposition of F-actin structures. The initial decrease of F-actin amount occured progressively between 2 and 20 h of the treatment (data not shown) and was completely insensitive to apoptosis inhibition (see the loss of MFI in imatinib + Q-VD-OPh samples compared to the controls in Fig. 2). On the other hand, the subsequent F-actin disassembly was fully prevented by 2 μM Q-VD-OPh (Fig. 2, bottom). Similar effect was achieved using zVADfmk at 50 μM, but not at 5 μM concentration, while zDEVDfmk had no effect on imatinib-induced actin depolymerization (data not shown, Table I).

CHANGES IN CELL ADHESIVITY TO FIBRONECTIN

The cell adhesivity to fibronectin was studied using the previously described protocol [Kuželová *et al.*, 2010]. The fraction of adhered cells was usually of 20–30% in the case of untreated JURL-MK1 cells under our experimental conditions. Imatinib mesylate treatment induced a moderate increase in the cell adhesivity during the first 6 h of the treatment (Fig. 3, the values for ACF are expressed as the

TABLE I. The Ability of Different Caspase Inhibitors to Inhibit the Observed Imatinib Mesylate-Induced Changes in JURL-MK1 Cells.

	5–50 μM zDEVDfmk, or 5 μM zVADfmk	50 μM zVADfmk	Q-VD-OPh (2 μM/10 μM)
Caspase-3 activation	++	++	++
DNA fragmentation	–	+	++
Necrosis	–	+	++
Actin depolymerization 1	–	–	–
Actin depolymerization 2	–	++	++
Decreased adhesivity to FN	–	–	+/++
Cofilin phosphorylation	–	n.d.	+
tropomyosin 1 decrease	n.d.	n.d.	+/++
Tropomyosin 4 decrease	n.d.	n.d.	–
ROCK cleavage	n.d.	–	–
LIMK decrease	n.d.	–	+
RhoGDI decrease	n.d.	n.d.	++
PAK-1 decrease	n.d.	n.d.	+
Paxillin decrease	n.d.	n.d.	+/++
Integrin β1 decrease	n.d.	n.d.	++
CD44 decrease	n.d.	n.d.	–

–, No effect; +, partial inhibition; ++, complete inhibition; n.d., not determined.
Actin depolymerization 1 and 2: moderate decrease of F-actin level within the first 20 h of Imatinib treatment and subsequent massive F-actin decomposition, respectively.

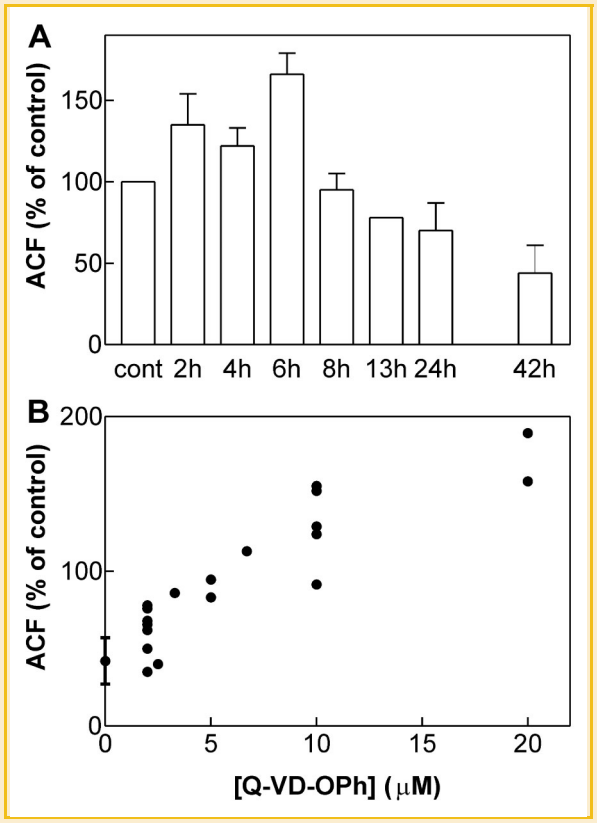

Fig. 3. JURL-MK1 adhesivity to fibronectin. Panel A: The cells were treated for up to 42 h (as indicated) with 1 μM imatinib mesylate, applied to fibronectin-coated microtitration plate and incubated for 1 h at 37°C. The ACF was then determined as described in Materials and Methods section and expressed as percentage of the untreated control. The plotted results represent means and standard deviation from 2 to 12 independent experiments. Panel B: Effect of simultaneous addition of Imatinib 1 μM and Q-VD-OPh at different concentrations on ACF. The point with error bars represents mean and standard deviation of ACF for cells treated with 1 μM imatinib only for 42–48 h (8 experiments). The other points correspond to samples treated with imatinib and Q-VD-OPh (2, 2.5, 3.3, 5, 6.7, 10, or 20 μM) for the same time intervals, the results are merged from several independent experiments.

percentage of the corresponding controls). Thereafter, the ACF progressively decreased to about a half of the control value after 42 h incubation. The loss of cell adhesivity was not affected by caspase inhibitors except for Q-VD-OPh, which displayed dose-dependent effects in the range of 2–20 μM concentrations (Fig. 3B).

2D-GEL ELECTROPHORESIS

The proteomic analysis of imatinib effects on JURL-MK1 cells was performed by means of 2D polyacrylamide gel electrophoresis (2D PAGE) in combination with mass spectrometry (MALDI-TOF). Fig. 4 shows the master map of JURL-MK1 cells and the identified proteins are listed in Table IS (Supplementary Material). An example of protein map obtained from cells treated with imatinib for 42 h is shown in Fig. 2S (Supplementary Material). By comparison of the protein maps obtained from control and imatinib-treated JURL-MK1 cells we found a reproducible increase in the intensity of the spots No 20 (cofilin), No 130 (stress-70 protein—GRP75) and No 147 (tropomyosin alpha-4, TPM4). Using a phosphopeptide-enriching GELoader microcolumn, we found that the spot No 20 contained the form of cofilin phosphorylated at Ser3. The intensity of several spots was systematically reduced by imatinib treatment: No 141 (deoxyuridine 5′-triphosphate nucleotidohydrolase), No 142 (nucleoside diphosphate kinase A), No 145 (proliferating cell nuclear antigen—PCNA), No 146 (elongation factor 1-beta), No 148 (tropomyosin alpha-3 chain), and Nos 149, 152, and 153 (14–3–3 proteins, isoforms epsilon, zeta/delta, and beta/alpha, respectively). The C-terminal cleavage of 14–3–3 proteins during imatinib-induced apoptosis has already been analyzed in our previous work [Kuželová *et al.*, 2009]. Among the other altered proteins, cofilin and tropomyosins are clearly related to the cytoskeleton architecture or cellular adhesion. We thus studied in detail their behavior after imatinib mesylate addition using specific antibodies: anti-cofilin, anti-phosphoSer3-cofilin, and anti-tropomyosins 1, 3, and 4.

COFILIN PHOSPHORYLATION DURING IMATINIB-INDUCED APOPTOSIS

While the expression level of cofilin displayed a mild decrease as a result of imatinib treatment (decrease to 82 ± 24%, mean and SD from four independent experiments), we observed a marked increase in the level of cofilin phosphorylation at Ser3 upon this treatment (Fig. 5A), which started as early as 2 h after imatinib addition (not shown). The average increase in cofilin phosphorylation after 42 h treatment was (7 ± 4) fold (mean and standard deviation from 13 independent experiments). Cofilin phosphorylation at Ser3 due to imatinib mesylate was at least partly inhibited by simultaneous addition of Q-VD-OPh: the increase in cofilin phosphorylation was reduced by (64 ± 27)% (mean and standard deviation from eight independent experiments) using 2 μM inhibitor (cf. lanes 4 and 5 in Fig. 5A). Increasing Q-VD-OPh concentration to 10 μM did not enhance the extent of the inhibition. The moderate imatinib-induced decrease in total cofilin level, if present, was also inhibited by Q-VD-OPh (Fig. 5A). We also tested the effect of Y-27632, a specific inhibitor of ROCK (Rho-associated kinase), which is a known upstream effector of cofilin phophorylation. The use of Y-27632 usually resulted in a decrease of cofilin phosphorylation in control JURL-MK1 cells (lane 3 in Fig. 5A) but this inhibitor had only minor effect on the pSer3-cofilin level in the cells treated with imatinib (lane 6 in Fig. 5A). Staining of 2D western blots by anti-pSer3-cofilin and anti-cofilin antibodies revealed a single spot corresponding to cofilin phosphorylated at Ser3 (probably the spot No 20 in Fig. 4) and two to three additional cofilin spots which are not recognized by the phospho-specific antibody (Fig. 5B). Thus, in spite of the increase in cofilin phosphorylation, a large pool of unphosphorylated cofilin is still present in imatinib-treated JURL-MK1 cells.

The intracellular localization of pSer3-cofilin and cofilin was studied by means of immunofluorescence microscopy. Both in the control and in imatinib-treated JURL-MK1 cells, p-cofilin was concentrated in small distinct areas, which were distributed throughout the cytoplasm (Fig. 6, upper panels). While the staining pattern did not essentially change after the treatment, the average cell fluorescence intensity corresponding to the labeled p-cofilin was higher in the treated cells. The histograms in Fig. 6 show the distribution of integrated fluorescence intensity from individual

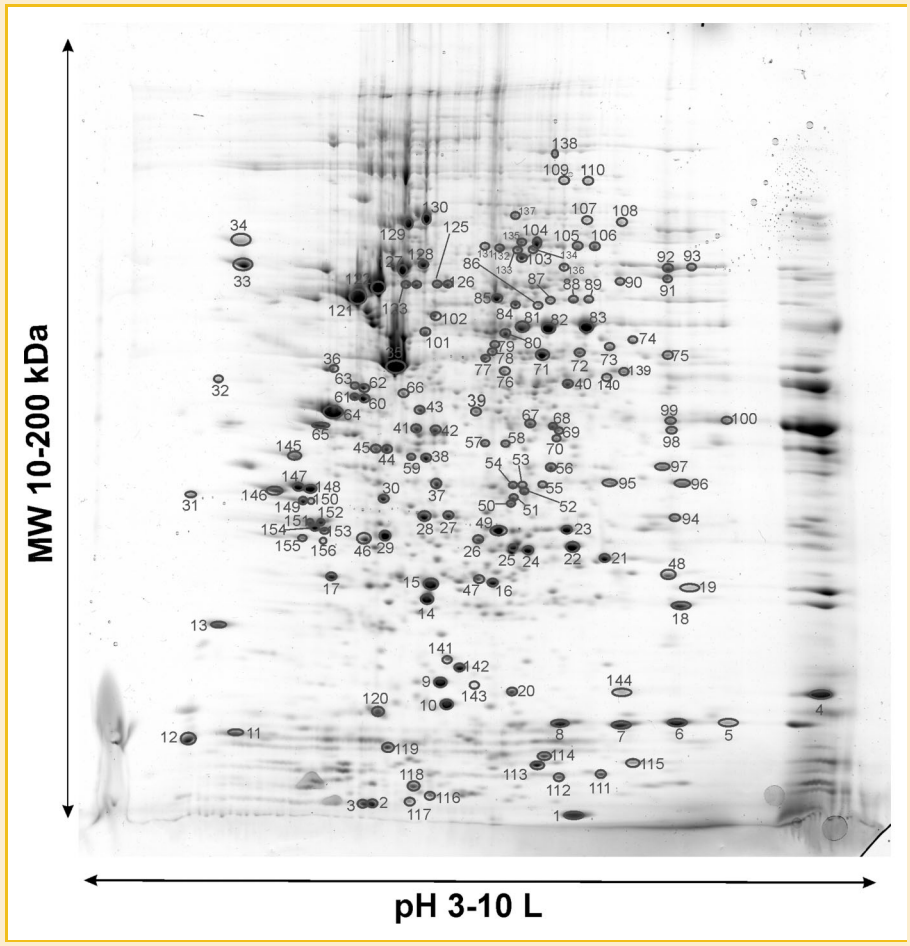

Fig. 4. Master map of JURL-MK1 cells. The protein mixture obtained from the whole cell lysates was resolved by isoelectric focusing followed by SDS electrophoresis. The gel was stained with Coomassie blue, the selected spots were excised from the gel and the proteins were identified using MALDI-TOF. The characterization of the numbered spots is given in Table IS (Supplementary Material).

cells for control (open symbols) and imatinib-treated (closed symbols) JURL-MK1 cells. When the cells where stained for total cofilin (independently of the phosphorylation status), we observed a rather diffuse signal which was localized mainly at the cell periphery in addition to the spotted pattern observed for phospho-cofilin (Fig. 6, lower right part).

CHANGES IN TROPOMYOSIN EXPRESSION LEVEL

Tropomyosins form part of actin filamentous structures and different tropomyosin isoforms are thought to be specifically involved in different types of actin filaments. Especially, high molecular weight (HMW) tropomyosins are associated with actin stress fiber formation while lower molecular weight (LMW) tropomyosins prevail in invasive cells. In 2D protein maps, we identified two spots containing LMW tropomyosin isoforms of TPM3 and TPM4, which were altered by imatinib mesylate treatment. Western blot analysis using specific antibodies did not confirm any consistent change in the expression levels of TPM3 while the amount of TPM4 was reduced by imatinib treatment (Fig. 5C). This decrease was insensitive to Q-VD-OPh addition. We also tested the level of HMW isoforms of TPM1, which are known to be implicated in stabilizing actin cytoskeleton filaments in non-muscle cells. We observed a decrease in the expression level of these isoforms following 24–48 h imatinib treatment which could be inhibited by Q-VD-OPh (Fig. 5C).

CHANGES IN KNOWN COFILIN REGULATORS

One of the most important regulation mechanisms of cofilin phosphorylation involves the kinases ROCK and their downstream effectors, LIM kinases (Fig. 3S, Supplementary Material). We thus explored their expression using specific antibodies. Imatinib mesylate induced cleavage of the protein ROCK1, which was insensitive to zVADfmk (up to 50 μM, not shown) and rather insensitive to Q-VD-OPh (up to 10 μM; Fig. 7). The results obtained with anti-LIMK1 and anti-phospho-LIMK1 antibodies were less conclusive: in different experiments, they ranged from no change to a large decrease both of the total protein level and of the phosphorylated form due to the imatinib treatment. The decrease, if present, was at least partly inhibited by 2 μM Q-VD-OPh (Fig. 7). Another protein, which is known to affect cofilin phosphorylation is PAK1 (p21-associated kinase 1, Fig. 3S). The level of PAK1 in JURL-MK1 cells markedly decreased as a result of imatinib mesylate

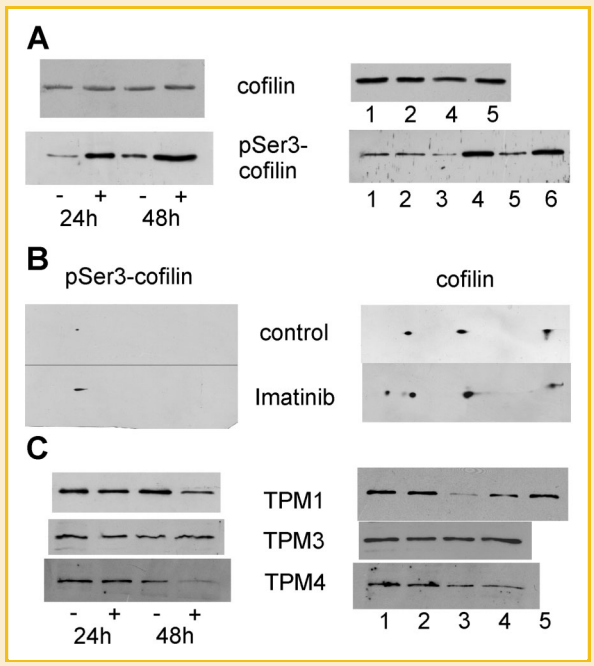

Fig. 5. Changes in cofilin and tropomyosin expression due to Imatinib treatment of JURL-MK1 cells. Panel A: Cofilin and pSer3-cofilin expression in JURL-MK1 cells cultivated for 24 or 48 h in the presence (+) or in the absence (−) of imatinib mesylate (left column) or incubated for 42 h with following agents: (1) control, (2) Q-VD-OPh 2 μM, (3) Y-27632 10 μM, (4) imatinib mesylate 1 μM, (5) imatinib with Q-VD-OPh, (6) imatinib with Y-27632. Panel B: 2D blots from control and imatinib-treated (1 μM, 42 h) cells using cofilin and pSer3-cofilin antibodies. Panel C: left: Expression of tropomyosin isoforms TPM1, TPM3, and TPM4 in cells cultivated for 24 or 48 h in the presence (+) or in the absence (−) of imatinib (left column) or incubated for 42 h with following agents: (1) control, (2) Q-VD-OPh 2 μM, (3) imatinib mesylate 1 μM, (4) imatinib with 2 μM Q-VD-OPh, (5) imatinib with 10 μM Q-VD-OPh.

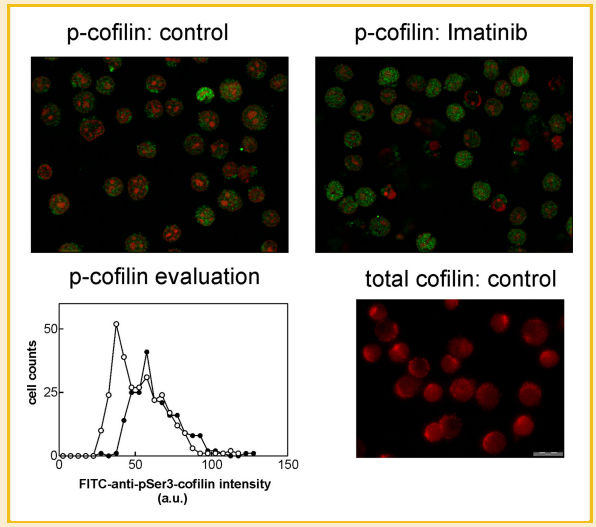

Fig. 6. Intracellular distribution of pSer3-cofilin and cofilin in JURL-MK1 cells. The control cells and the cells treated with 1 μM imatinib mesylate for 40 h were fixed, permeabilized and stained with anti-pSer3-cofilin (upper panels) or anti-cofilin (lower right panel) antibody and subsequently with FITC-labeled (green) or PE-labeled (red) secondary antibody, respectively. In the upper panels, the cell nuclei were stained with propidium iodide (red). The pictures were enregistred using Olympus IX81 microscope with Cell-R system, magnification 60×. Lower left part: Histograms of FITC-fluorescence intensity from anti-pSer3-cofilin-labeled control (open symbols) and imatinib-treated (closed symbols) cells. The green fluorescence intensity from individual cells was evaluated using Phoretix™ 2D Expression software. The experiment was repeated with similar results.

treatment and the decrease was partly reversible by Q-VD-OPh. The expression level of RhoGDI, a negative regulator of Rho GTPase activity, was also largely reduced by imatinib treatment and this effect was reversed by 2 μM Q-VD-OPh.

CHANGES IN SURFACIAL PROTEIN EXPRESSION

The cell adhesion to the proteins of the ECM is mainly mediated by integrins. In a previous work, we identified integrin β1 as the most important interaction partner for fibronectin in the case of JURL-MK1 cells [Kuželová *et al.*, 2010]. We used a PE-labeled anti-integrin β1 antibody to study the amount of this integrin at the surface of JURL-MK1 cells by means of flow-cytometry. The scattergrams presented in Fig. 8 reveal the presence of a cell subpopulation with altered scattering properties (especially with lower FSC indicating smaller cell size) in the imatinib-treated sample. Q-VD-OPh inhibits these imatinib-induced changes in the cell size and shape (Fig. 8, left panels C and D; we also made the same conclusion from the microscopic observation of cell preparations: Fig. 4S in Supplementary Material). Presumably, the observed morphological changes correspond to cell shrinking and membrane blebbing which are known to occur as a part of the apoptosis. Indeed, imatinib treatment leads to a large increase in Annexin-positive cell fraction and the majority of Annexin-positive cells are found in the region denoted as Alt (Fig. 5S, Supplementary Material). As it is shown in Fig. 8, the cells with altered morphology (i.e., apoptotic) display lowered surfacial expression of integrin β1 and the decrease in anti-integrin staining can be reversed by simultaneous addition of Q-VD-OPh.

Changes in the expression level of some other adhesion molecules have been previously reported to occur in CML cells and we thus analyzed the surfacial expression level of hyaluronic acid receptor (HCAM, CD44) and those of P and L-selectin (CD62P and CD62L). We observed about 50% reduction in PE-anti-CD44 staining due to 42 h imatinib treatment. This decrease occurred both in "normal" and "altered" subpopulations and was almost insensitive to Q-VD-OPh addition (Fig. 6S, Supplementary Material). On the other hand, neither control nor imatinib-treated JURL-MK1 cells were significantly labeled with anti-CD62 antibodies indicating that JURL-MK1 cells do not express selectins on their surface.

CHANGES IN PAXILLIN EXPRESSION LEVEL

During the cell adhesion, the integrins cluster and large protein complexes (so-called focal adhesions) are formed at their cytoplasmic tails. An important component of these complexes is the protein paxillin and labeled anti-paxillin antibodies are often used to stain focal adhesions for microscopic observations. We examine paxillin expression level using Western blotting and found

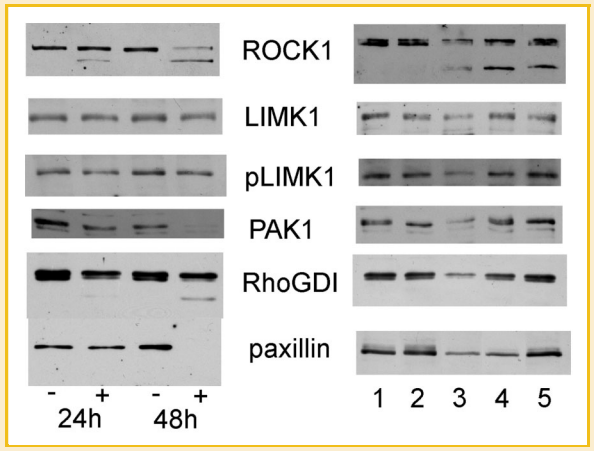

Fig. 7. Changes in protein expression levels induced by imatinib treatment in JURL-MK1 cells. Left column: Cells were incubated in the absence (−) or in the presence (+) of 1 μM imatinib mesylate for 24–48 h as indicated. Right column: Cells were incubated with 1 μM imatinib, Q-VD-OPh or with their combination for 42 h. The expression level of the specified proteins was assessed by Western blotting. Lane 1: control, lane 2: Q-VD-OPh, lane 3: imatinib mesylate, lanes 4 and 5: imatinib mesylate in combination with Q-VD-OPh 2 μM (4) or 10 μM (5).

that it was lowered due to imatinib treatment of JURL-MK1 cells. The inhibitor Q-VD-OPh was able to prevent this decrease in a dose-dependent manner similar to that observed for the decrease of the cell adhesivity to fibronectin: the effect was only modest at 2 μM Q-VD-OPh but complete inhibition was achieved using 10 μM Q-VD-OPh (Fig. 7, Table I).

The summary of the effect of caspase inhibitors on the individual changes occuring as a result of imatinib mesylate treatment of JURL-MK1 cells is given in Table I.

DISCUSSION

Altered adhesivity to the ECM is one of the characteristic features of CML, which is manifested by an expansion of myeloid cells and their premature release into the peripheral blood. The fusion protein Bcr–Abl which is the molecular cause of the disease, affects at multiple points the pathways leading from focal adhesions to the cytoskeleton [Kuželová and Hrkal, 2008]. The inhibition of Bcr–Abl tyrosine-kinase activity by imatinib mesylate eventually results in Bcr–Abl degradation (Fig. 1S, Supplementary Material) and presumably changes the activation state of the focal adhesion pathways. In parallel, imatinib mesylate induces apoptosis and the focal adhesion pathways can thus also be modulated as a part of apoptosis execution. Many structural and regulatory proteins which are involved in the cell adhesivity and cytoskeleton dynamics are substrates for caspases and caspase-mediated proteolysis is believed to contribute to focal adhesion disassembly, cell detachment from the ECM and the eventual cell collapse. We have previously shown that the treatment of JURL-MK1 cells with 1 μM imatinib mesylate triggers caspase-3 activation (reaching the maximum after about 40 h of treatment), apoptotic DNA fragmentation and cell death in the whole cell population [Kuželová *et al.*, 2005]. In the attempt to discriminate between primary and secondary effects of imatinib on JURL-MK1 cell adhesion signaling, we employed three different caspase inhibitors in combination with imatinib. All these inhibitors were able to suppress imatinib-induced activation of caspase-3 measured in an in vitro assay, even at concentrations lower than 2 μM (Fig. 1A). We also verified by anti-caspase-3 Western blotting that the inhibitors irreversibly bound to virtually all caspase-3 molecules under these conditions (see Kuželová *et al.*, 2007 for zDEVDfmk and zVADfmk, we performed similar experiments for Q-VD-OPh, data not shown). Anti-caspase-3 Western blots also showed that the inhibitors interfere with pro-caspase-3 processing and prevent the formation of the active caspase-3 at concentrations up from 0.5 μM. On the other hand, the individual inhibitors largely differ in their ability to prevent other apoptotic processes, such as DNA fragmentation (Fig. 1B). These results show that other proteins than caspase-3 must be involved in the execution of JURL-MK1 cell apoptosis induced by imatinib mesylate and these pathways are blocked by Q-VD-OPh.

Our experimental results show that the actin cytoskeleton of JURL-MK1 cells undergoes massive and complex rearrangements as a result of imatinib treatment. It is likely that the majority of F-actin fibres are progressively decomposed in relation with the proceeding apoptosis. The massive disruption can be prevented by caspase inhibitors zVADfmk (at 50 μM, data not shown) and Q-VD-OPh (Fig. 2), but not by zDEVDfmk at up to 50 μM concentration (data not shown, Table I). Caspase-3 is thus not the key player in this event. In addition, the early mild but homogeneous decrease in F-actin amount indicated by the decrease in MFI in Fig. 2 cannot be inhibited by any of the inhibitor used. This change may thus either be part of very early apoptotic processes (upstream of the activation of caspases or other proteases which are targeted by the inhibitors) or may result directly from the inhibition of Bcr–Abl signaling through cytoskeleton-regulating pathways.

JURL-MK1 cell adhesivity to fibronectin-coated surface was measured using the previously described sensitive assay with fluorescence detection (Fig. 3A). The initial moderate increase in the ACF during the first 6 h of imatinib treatment is probably directly due to the switch-off of Bcr–Abl action on the adhesion signaling pathways. We propose that this change is later overbalanced by apoptosis-related decrease in the cell adhesivity as the net decrease of ACF after 42 h Imatinib treatment was fully reversed using 10 μM Q-VD-OPh (Fig. 3B). While both the F-actin decomposition and the decrease in cellular adhesivity probably occur as integral parts of the apoptosis, the underlying mechanisms are not the same as they differ in their sensitivity to zVADfmk and Q-VD-OPh (Table I, Figs. 2 and 3). On the other hand, we observed a nice correlation as to the effects of Q-VD-OPh on the loss of JURL-MK1 cell adhesivity and on the decrease of the expression level of paxillin (cf. Figs. 3 and 7). This finding is consistent with the important role of the protein paxillin in the function of focal adhesion complexes and indicates that imatinib-induced decrease in paxillin level might be at least partly responsible for the loss of focal adhesion function. However, paxillin decrease is not due to caspase-3 activity (and probably not due to any other caspase) as 10 μM Q-VD-OPh is required to block this consequence of imatinib treatment while all the tested caspase

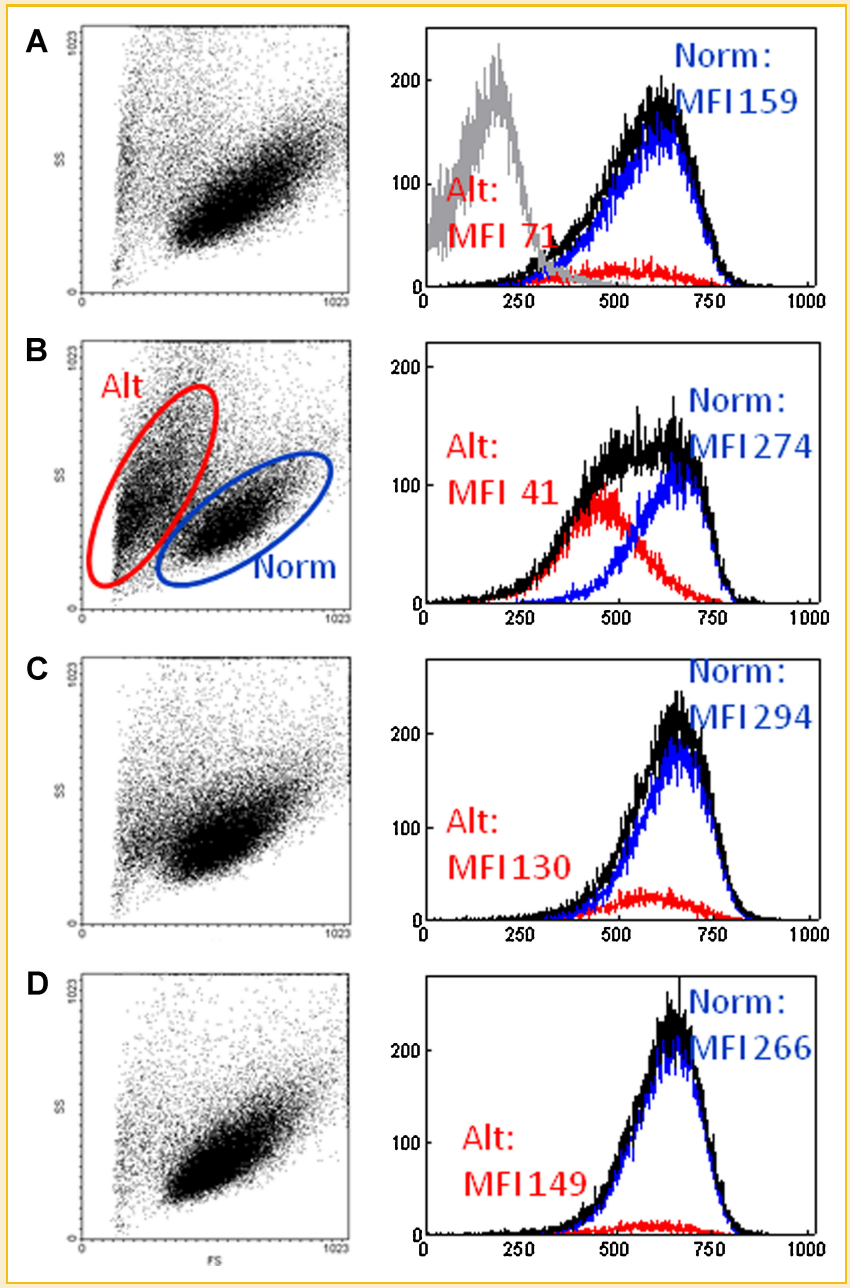

Fig. 8. Changes in surfacial integrin β1 expression due to imatinib mesylate treatment of JURL-MK1 cells. The cells were treated for 48 h with 1 μM imatinib alone or in combination with 2 μM Q-VD-OPh, labeled with PE-conjugated anti-β1 integrin and analyzed by means of flow cytometry. Left part: scattergrams (FSC—forward scatter, SSC—side scatter) with indicated gating regions for cells with normal (Norm) and altered (Alt) scattering properties. Right part: histograms of PE fluorescence intensity for all cells and for cells gated in regions Norm (blue) and Alt (red). MFI indicates the corresponding mean fluorescence intensity. A: untreated control (negative control without staining is shown on the left side of the histogram), B: imatinib mesylate, C: imatinib + 2 μM Q-VD-OPh, D: imatinib + 10 μM Q-VD-OPh. The negative control (i.e., no staining) is shown on the left side (gray line) of the upper histogram.

inhibitors at 0.5 μM concentration were able to prevent the caspase-3 activity.

We also found that imatinib mesylate treatment reduced the amount of integrin β1 on the surface of JURL-MK1 cells. The decrease was observed in cells with altered scattering properties (Fig. 8, lower FSC and slightly higher SSC indicate decreased cell size and increased granularity in the cell subpopulation denoted as Alt). As confirmed by Annexin staining, these morphological changes probably occur in relation with the apoptosis (Fig. 5S). As integrin β1 is the most important interaction partner for fibronectin, its lowered expression can contribute to the observed decrease in the cell adhesivity. However, the decrease in integrin β1 expression was largely prevented by 2 μM Q-VD-OPh (Fig. 8) whereas higher concentration of Q-VD-OPh (10 μM, Fig. 3) was required to restore the cell adhesivity. The partial loss of integrin β1 staining is thus not the major cause for the loss of the cell adhesivity and rather

represents a consequence of cell surface modification due to the apoptotic cell shrinking.

It was reported that the adhesion molecule CD44, a glycoprotein which is involved in the primary adhesion of lymphocytes to endothelial cells as well as in cell interaction with ECM, is required in homing of Bcr–Abl-expressing mouse leukemic stem cells [Krause *et al*., 2006] and that an increase in CD44 expression was associated with acquired resistance to imatinib in K562 cell line [Grosso *et al*., 2009]. We searched for potential changes in CD44 expression on JURL-MK1 cell surface upon imatinib treatment and confirmed that CD44 expression was reduced by imatinib independently of Q-VD-OPh addition (Fig. 6S, Supplementary Material). Thus, imatinib mesylate is likely to affect the primary adhesion of CML cells to the endothelial cells and the migration of hematopoietic stem cells to the bone marrow during the transplantation.

Imatinib was also reported to restore impared CD62L expression in CML cells [Fruehauf *et al*., 2003] but we did not detect any change in very weak anti-selectin (both CD62L and CD62P) staining of JURL-MK1 cells upon imatinib treatment.

The proteomic analysis of imatinib effects revealed an increased phophorylation of cofilin at Ser3 (Fig. 5A). Cofilin is the pivotal mediator of actin dynamics, which promotes actin filament severing and depolymerization, facilitating the breakdown of existing filaments, and the enhancement of filament growth from newly created barbed ends [DesMarais et al., 2005; Burkhardt et al., 2008; Van Troys et al., 2008; van Rheenen et al., 2009]. It is involved in many processes, which include cytoskeletal rearrangements, such as mitosis, cytokinesis, cell migration, or cell adhesion and it was also reported to be required for cytochrome c release during mitochondrial apoptosis [Chua *et al*., 2003; Zhu *et al*., 2006]. Phosphorylation of cofilin at Ser3 is known to prevent its actin-depolymerization activity. For example, cofilin is present in its inactive/phosphorylated form in human peripheral blood T-lymphocytes and is activated upon their stimulation, which involves dynamic rearrangements of the actin cytoskeleton [Samstag and Nebl, 2005]. Cofilin is also activated during HIV infection of T-cells and helps the virus to overcome the static cortical actin restriction [Yoder *et al*., 2008].

The increased phosphorylation of cofilin due to imatinib mesylate treatment of JURL-MK1 cells was indicated by the analysis of 2D protein maps (increased intensity of the spot No 20 in Fig. 4 which was identified as phosphorylated cofilin) and subsequently confirmed by means of Western blotting using phosphoSer3-specific antibody (Fig. 5A). An increase in phospho-cofilin staining intensity was detected also when the staining was performed on fixed and permeabilized whole cells and analyzed using a microscope (Fig. 6). The difference in the intensity of staining between control and treated cells was less marked in microscopic analysis (about twofold increase in phosphorylation) in comparison with Western blot analysis (about sevenfold increase), but this discrepancy can be due to lower accessibility of the epitope in the whole cell environment. Indeed, the microscopic analysis shows that phosphorylated cofilin is mainly located in cytoplasmic foci where it is likely to form complexes with other proteins such as 14–3–3s [Liang *et al*., 2009]. Redistribution of cofilin into similar punctuated pattern has been previously observed by others, for example, after siRNA-mediated knock-down of cyclase-associated protein 1 (CAP1) that colocalizes with cofilin-1 to dynamic regions of the cortical actin cytoskeleton and promotes actin filament depolymerization [Bertling *et al*., 2004]. Although the authors did not look at cofilin phosphorylation status, we presume that the translocated cofilin fraction may have been phosphorylated (inactivated) as CAP1 depletion led to similar cytoskeletal defects as cofilin knock-down.

The extensive F-actin decomposion occuring after JURL-MK1 cell treatment with imatinib mesylate could be due to an increased cofilin activity, which should be accompanied by a decrease in cofilin phosphorylation. The actual observation (a marked increase in cofilin phosphorylation) thus seems to be controversial. It is tempting to speculate, however, that some prominent F-actin structures have to be protected to assure the controlled cell disintegration into apoptotic bodies. Cofilin phosphorylation/inactivation in the vicinity of these structures could thus be an integral part of the programmed cell death. Indeed, the increase in cofilin phosphorylation at Ser3 occurring after imatinib treatment of JURL-MK1 cells can be at least partly suppressed by Q-VD-OPh (Fig. 5A). Our results are in line with those of Song et al. (2002) who reported that the expression of constitutively activated form of cofilin (unphosphorylatable at Ser3) suppressed both membrane blebbing and chromatin condensation in ROCK-expressing cells. On the other hand, cofilin dephosphorylation/activation was observed during H_2O_2-induced apoptosis of vascular smooth muscle cells [Lee *et al*., 2006].

One of the major mechanisms of cofilin regulation involves the proteins ROCK, downstream effectors of RhoA GTPase (Fig. 3S). ROCK1 was reported to be constitutively activated through the cleavage of its autoinhibitory tail by caspase-3 [Coleman *et al*., 2001] and is believed to play an essential role in morphological changes associated with the apoptosis [Coleman and Olson, 2002; Song *et al*., 2002]. ROCK inhibition also impedes multiple myeloma cell homing to the bone marrow [Azab *et al*., 2009]. We indeed observed ROCK1 cleavage (though not attributable to caspase-3 as any of caspase inhibitors used did not prevent the cleavage) during imatinib-induced apoptosis of JURL-MK1 cells (Fig. 7). We thus searched for possible effects of Y-27632, a specific inhibitor of ROCK1 and ROCK2. In control JURL-MK1 cells, Y-27632 (10 μM) decreased the level of cofilin phosphorylation (Fig. 5A, lane 3) and slighty reduced the intensity of F-actin staining with phalloidin (decrease in MFI was 10–15% after 24 h and the effect was not enhanced at higher Y-27632 concentration, data not shown). The inhibitor Y-27632 at this usually used concentration was thus probably efficient in ROCK inhibition, but despite this it did not significantly reduce imatinib-induced phosphorylation of cofilin (Fig. 5A, lane 6). ROCK is thus probably not the protein mediating cofilin phosphorylation during imatinib-induced apoptosis of JURL-MK1 cells. In line with this conclusion, we observed no increase in phosphorylation (i.e., no activation) of LIM kinase (Fig. 7), which is known to mediate the effect of ROCK on cofilin [Tomiyoshi et al., 2004; Scott and Olson, 2007]. Besides the pathway RhoA/ROCK/LIMK, multiple other mechanisms can contribute to the regulation of cofilin phosphorylation. These involve several p21-activated kinases (PAKs) [Coniglio *et al*., 2008; Pandey *et al*., 2009], integrin-linked kinase (ILK, [Kim *et al*., 2008]), cofilin-specific

phosphatases [Huang et al., 2006; Eiseler et al., 2009; Kim et al., 2009], or actin-interactin protein 1 (Aip1), which works in cooperation with caspase-11 to promote cofilin-mediated actin depolymerization [Li *et al.*, 2007]. In our experimental system, the observed reduction in PAK1 level induced by imatinib mesylate (Fig. 7) could contribute to the increased cofilin phosphorylation as the activation of this kinase was reported to result in cofilin dephosphorylation [Coniglio *et al.*, 2008].

Spatially, the activity of cofilin is restricted by other actin-binding proteins, such as tropomyosins, which competes for accessibility of actin filament populations in different regions of the cell [DesMarais *et al.*, 2005; Fan *et al.*, 2008]. Tropomyosins are coiled-coil dimers that form continuous polymers along the major groove of most actin filaments. Different tropomyosin isoforms interact with different actin-binding proteins such as cofilin, Arp 2/3, or myosin and thereby confer different properties to the actin filaments [Gunning *et al.*, 2008; Kuhn and Bamburg, 2008]. Although the function of the individual tropomyosin isoforms is not well understood, the HMW isoforms of TPM1 are thought to increase the stability of actin stress fibers [Gunning *et al.*, 2008]. The reduced level of TPM1, which we found in imatinib-treated JURL-MK1 cells (Fig. 5C) thus could contribute to imatinib induced F-actin disassembly (Fig. 2).

ACKNOWLEDGMENTS

We wish to thank H. Pilcová, J. Sedlmaierová, and M. Voráčová for the expert technical assistance and O. Šebesta from the Faculty of Science of Charles University in Prague for taking the pictures from the fluorescence microscope. The authors apologize to all colleagues whose work could not be cited due to space limitation. This work was suppported by Ministry of Health of the Czech Republic NR 9243-3 and VZ 00023736 (to K.K., M.P., D.G., and Z.H.), Ministry of Education, Youth and Sports of the Czech Republic LC 07017 and AV0Z50200510 (to P.H. and K.P.).

REFERENCES

Azab AK, Azab F, Blotta S, Pitsillides CM, Thompson B, Runnels JM, Roccaro AM, Ngo HT, Melhem MR, Sacco A, Jia X, Anderson KC, Lin CP, Rollins BJ, Ghobrial IM. 2009. RhoA and Rac1 GTPases play major and differential roles in stromal cell-derived factor-1-induced cell adhesion and chemotaxis in multiple myeloma. Blood 114:619–629.

Barnes DJ, Schultheis B, Adedeji S, Melo JV. 2005. Dose-dependent effects of bcr-abl in cell line models of different stages of chronic myeloid leukemia. Oncogene 24:6432–6440.

Bazzoni G, Carlesso N, Griffin JD, Hemler ME. 1996. Bcr/Abl expression stimulates integrin function in hematopoietic cell lines. J Clin Invest 98:521–528.

Bertling E, Hotulainen P, Mattila PK, Matilainen T, Salminen M, Lappalainen P. 2004. Cyclase-associated protein 1 (CAP1) promotes cofilin-induced actin dynamics in mammalian nonmuscle cells. Mol Biol Cell 15:2324–2334.

Bhatia R, Verfaillie CM. 1998. Inhibition of BCR-ABL expression with antisense oligodeoxynucleotides restores beta1 integrin-mediated adhesion and proliferation inhibition in chronic myelogenous leukemia hematopoietic progenitors. Blood 91:3414–3422.

Burkhardt JK, Carrizosa E, Shaffer MH. 2008. The actin cytoskeleton in T cell activation. Annu Rev Immunol 26:233–259.

Cheng K, Kurzrock R, Qiu X, Estrov Z, Ku S, Dulski KM, Wang JY, Talpaz M. 2002. Reduced focal adhesion kinase and paxillin phosphorylation in BCR-ABL-transfected cells. Cancer 95:440–450.

Chua BT, Volbracht C, Tan KO, Li R, Yu VC, Li P. 2003. Mitochondrial translocation of cofilin is an early step in apoptosis induction. Nat Cell Biol 5:1083–1089.

Coleman ML, Olson MF. 2002. Rho GTPase signalling pathways in the morphological changes associated with apoptosis. Cell Death Differ 9:493–504.

Coleman ML, Sahai EA, Yeo M, Bosch M, Dewar A, Olson MF. 2001. Membrane blebbing during apoptosis results from caspase-mediated activation of ROCK I. Nat Cell Biol 3:339–345.

Coniglio SJ, Zavarella S, Symons MH. 2008. Pak1 and Pak2 mediate tumor cell invasion through distinct signaling mechanisms. Mol Cell Biol 28:4162–4172.

Dai Y, Rahmani M, Corey SJ, Dent P, Grant S. 2004. A Bcr/Abl-independent, lyn-dependent form of imatinib mesylate (STI-571) resistance is associated with altered expression of bcl-2. J Biol Chem 279:34227–34239.

DesMarais V, Ghosh M, Eddy R, Condeelis J. 2005. Cofilin takes the lead. J Cell Sci 118:19–26.

Eiseler T, Doppler H, Yan IK, Kitatani K, Mizuno K, Storz P. 2009. Protein kinase D1 regulates cofilin-mediated F-actin reorganization and cell motility through slingshot. Nat Cell Biol 11:545–556.

Fan X, Martin-Brown S, Florens L, Li R. 2008. Intrinsic capability of budding yeast cofilin to promote turnover of tropomyosin-bound actin filaments. PLoS One 3:e3641. DOI: 10.1371/journal.pone.0003641.

Fruehauf S, Topaly J, Schad M, Paschka P, Gschaidmeier H, Zeller WJ, Hochhaus A, Ho AD. 2003. Imatinib restores expression of CD62L in BCR-ABL-positive cells. J Leukoc Biol 73:600–603.

Gaston I, Stenberg PE, Bhat A, Druker BJ. 2000. Abl kinase but not PI3-kinase links to the cytoskeletal defects in bcr-abl transformed cells. Exp Hematol 28:351.

Goldman JM, Melo JV. 2003. Chronic myeloid leukemia—Advances in biology and new approaches to treatment. N Engl J Med 349:1451–1464.

Grosso S, Puissant A, Dufies M, Colosetti P, Jacquel A, Lebrigand K, Barbry P, Deckert M, Cassuto JP, Mari B, Auberger P. 2009. Gene expression profiling of imatinib and PD166326-resistant CML cell lines identifies fyn as a gene associated with resistance to BCR-ABL inhibitors. Mol Cancer Ther 8:1924–1933.

Gunning P, O'Neill G, Hardeman E. 2008. Tropomyosin-based regulation of the actin cytoskeleton in time and space. Physiol Rev 88:1–35.

Huang TY, DerMardirossian C, Bokoch GM. 2006. Cofilin phosphatases and regulation of actin dynamics. Curr Opin Cell Biol 18:26–31.

Kim YB, Choi S, Choi MC, Oh MA, Lee SA, Cho M, Mizuno K, Kim SH, Lee JW. 2008. Cell adhesion-dependent cofilin serine 3 phosphorylation by the integrin-linked kinase.c-src complex. J Biol Chem 283:10089–10096.

Kim JS, Huang TY, Bokoch GM. 2009. Reactive oxygen species regulate a slingshot-cofilin activation pathway. Mol Biol Cell 20:2650–2660.

Kramer A, Horner S, Willer A, Fruehauf S, Hochhaus A, Hallek M, Hehlmann R. 1999. Adhesion to fibronectin stimulates proliferation of wild-type and bcr/abl-transfected murine hematopoietic cells. Proc Natl Acad Sci USA 96:2087–2092.

Krause DS, Lazarides K, von Andrian UH, Van Etten RA. 2006. Requirement for CD44 in homing and engraftment of BCR-ABL-expressing leukemic stem cells. Nat Med 12:1175–1180.

Kuhn TB, Bamburg JR. 2008. Tropomyosin and ADF/cofilin as collaborators and competitors. Adv Exp Med Biol 644:232–249.

Kuželová K, Hrkal Z. 2008. Rho-signaling pathways in chronic myelogenous leukemia. Cardiovasc Hematol Disord Drug Targets 8:261–267.

Kuželová K, Grebeňová D, Marinov I, Hrkal Z. 2005. Fast apoptosis and erythroid differentiation induced by imatinib mesylate in JURL-MK1 cells. J Cell Biochem 95:268–280.

Kuželová K, Grebeňová D, Hrkal Z. 2007. Labeling of apoptotic JURL-MK1 cells by fluorescent caspase-3 inhibitor FAM-DEVD-fmk occurs mainly at site(s) different from caspase-3 active site. Cytometry A 71:605–611.

Kuželová K, Grebeňová D, Pluskalová M, Kavan D, Halada P, Hrkal Z. 2009. Isoform-specific cleavage of 14–3–3 proteins in apoptotic JURL-MK1 cells. J Cell Biochem 106:673–681.

Kuželová K, Pluskalová M, Brodská B, Otevřelová P, Elknerová K, Grebeňová D, Hrkal Z. 2010. Suberoylanilide hydroxamic acid (SAHA) at subtoxic concentrations increases the adhesivity of human leukemic cells to fibronectin. J Cell Biochem 109:184–195.

Larsen MR, Thingholm TE, Jensen ON, Roepstorff P, Jorgensen TJ. 2005. Highly selective enrichment of phosphorylated peptides from peptide mixtures using titanium dioxide microcolumns. Mol Cell Proteomics 4:873–886.

Lee CK, Park HJ, So HH, Kim HJ, Lee KS, Choi WS, Lee HM, Won KJ, Yoon TJ, Park TK, Kim B. 2006. Proteomic profiling and identification of cofilin responding to oxidative stress in vascular smooth muscle. Proteomics 6:6455–6475.

Li J, Brieher WM, Scimone ML, Kang SJ, Zhu H, Yin H, von Andrian UH, Mitchison T, Yuan J. 2007. Caspase-11 regulates cell migration by promoting Aip1-cofilin-mediated actin depolymerization. Nat Cell Biol 9:276–286.

Liang S, Yu Y, Yang P, Gu S, Xue Y, Chen X. 2009. Analysis of the protein complex associated with 14–3–3 epsilon by a deuterated-leucine labeling quantitative proteomics strategy. J Chromatogr B Analyt Technol Biomed Life Sci 877:627–634.

Pandey D, Goyal P, Dwivedi S, Siess W. 2009. Unraveling a novel Rac1-mediated signaling pathway that regulates cofilin dephosphorylation and secretion in thrombin-stimulated platelets. Blood 114:415–424.

Ramaraj P, Singh H, Niu N, Chu S, Holtz M, Yee JK, Bhatia R. 2004. Effect of mutational inactivation of tyrosine kinase activity on BCR/ABL-induced abnormalities in cell growth and adhesion in human hematopoietic progenitors. Cancer Res 64:5322–5331.

Salesse S, Verfaillie CM. 2002. Mechanisms underlying abnormal trafficking and expansion of malignant progenitors in CML: BCR/ABL-induced defects in integrin function in CML. Oncogene 21:8605–8611.

Salgia R, Li JL, Ewaniuk DS, Pear W, Pisick E, Burky SA, Ernst T, Sattler M, Chen LB, Griffin JD. 1997. BCR/ABL induces multiple abnormalities of cytoskeletal function. J Clin Invest 100:46–57.

Samstag Y, Nebl G. 2005. Ras initiates phosphatidyl-inositol-3-kinase (PI3K)/PKB mediated signalling pathways in untransformed human peripheral blood T lymphocytes. Adv Enzyme Regul 45:52–62.

Scott RW, Olson MF. 2007. LIM kinases: Function, regulation and association with human disease. J Mol Med 85:555–568.

Song Y, Hoang BQ, Chang DD. 2002. ROCK-II-induced membrane blebbing and chromatin condensation require actin cytoskeleton. Exp Cell Res 278:45–52.

Tomiyoshi G, Horita Y, Nishita M, Ohashi K, Mizuno K. 2004. Caspase-mediated cleavage and activation of LIM-kinase 1 and its role in apoptotic membrane blebbing. Genes Cells 9:591–600.

van Rheenen J, Condeelis J, Glogauer M. 2009. A common cofilin activity cycle in invasive tumor cells and inflammatory cells. J Cell Sci 122:305–311.

Van Troys M, Huyck L, Leyman S, Dhaese S, Vandekerkhove J, Ampe C. 2008. Ins and outs of ADF/cofilin activity and regulation. Eur J Cell Biol 87:649–667.

Vega FM, Ridley AJ. 2008. Rho GTPases in cancer cell biology. FEBS Lett 582:2093–2101.

Wertheim JA, Forsythe K, Druker BJ, Hammer D, Boettiger D, Pear WS. 2002. BCR-ABL-induced adhesion defects are tyrosine kinase-independent. Blood 99:4122–4130.

Wertheim JA, Perera SA, Hammer DA, Ren R, Boettiger D, Pear WS. 2003. Localization of BCR-ABL to F-actin regulates cell adhesion but does not attenuate CML development. Blood 102:2220–2228.

Yoder A, Yu D, Dong L, Iyer SR, Xu X, Kelly J, Liu J, Wang W, Vorster PJ, Agulto L, Stephany DA, Cooper JN, Marsh JW, Wu Y. 2008. HIV envelope-CXCR4 signaling activates cofilin to overcome cortical actin restriction in resting CD4 T cells. Cell 134:782–792.

Zandy NL, Playford M, Pendergast AM. 2007. Abl tyrosine kinases regulate cell-cell adhesion through rho GTPases. Proc Natl Acad Sci USA 104:17686–17691.

Zhao RC, Jiang Y, Verfaillie CM. 2001. A model of human p210(bcr/ABL)-mediated chronic myelogenous leukemia by transduction of primary normal human CD34(+) cells with a BCR/ABL-containing retroviral vector. Blood 97:2406–2412.

Zhu B, Fukada K, Zhu H, Kyprianou N. 2006. Prohibitin and cofilin are intracellular effectors of transforming growth factor beta signaling in human prostate cancer cells. Cancer Res 66:8640–8647.